Chemical Physics Impact 2 (2021) 100014

Contents lists available at ScienceDirect

Chemical Physics Impact

journal homepage: www.elsevier.com/locate/chphi

Silver nanoparticle aggregates: Wavelength dependence of their SERS properties in the first transparency window of biological tissues

Roberto Pilot[a,b,*], Michele Massari[b,c,#]

[a] Consorzio INSTM, Via G. Giusti 9, 50121 Firenze, Italy
[b] Department of Chemical Sciences, University of Padova, Via Marzolo 1, 35131 Padova, Italy
[c] LaNN Laboratory for Nanofabrication of Nanodevices, Veneto Nanotech s.c.p.a., Corso Stati Uniti 4, 35127 Padova, Italy

ARTICLE INFO

Keywords:
Raman
SERS
Surface enhanced
Silver nanoparticles
Aggregates

ABSTRACT

Silver nanoparticle aggregates are very common substrates for surface enhanced Raman scattering (SERS) due to their simplicity of preparation and good optical enhancement. In this paper, their SERS properties are investigated from 680 to 920 nm, region that spans most of the first transparency window of biological tissues.

Our experiments show that the SERS enhancement extends as far as 920 nm, without a significant wavelength dependence: the observed very broad optical response has been interpreted with the formation of large sized aggregates, possibly possessing a partial fractal character. On the other hand, the SERS signal, normalized by the laser power and by the integration time, quickly diminishes from 680 to 920 nm. This happens because the SERS signal depends on the enhancement but also on the instrument sensitivity and on the molecular cross section: for dispersive Raman instruments equipped with silicon CCD detectors and for non resonant molecules, these two parameters tend to diminish towards longer excitation wavelengths.

The relevance of these results is twofold. a) Simple silver nanoparticle aggregates are good plasmonic substrates in most of the spectral region in which biological tissues present low absorption. b) The enhancement of the substrate and the normalized SERS signal (that is related to the limit of detection) are not necessarily correlated: they carry complementary pieces of information, both needed for properly designing a SERS experiment.

1. Introduction

Surface enhanced Raman scattering (SERS) has emerged in the last decades as an important tool for the detection of analytes at very low concentration in different contexts [1–3]. Examples include the detection of food contaminants [4,5], explosives [6–8], environmental pollutants [9,10], natural or synthetic substances in the field of art preservation [11], biomolecules [12–14], bacteria [15], cells [16,17], and catalytic intermediates [18,19]. The fabrication and characterization of substrates with optimal features for SERS is crucial to the development and to the widespread diffusion of this technique.

In order to evaluate the SERS performance, the enhancement (G_{SERS}) is commonly used as a figure of merit [20,21]. It essentially depends on the characteristics of the substrate, in particular the type of material and the morphology.[1] Often, also the limit of detection (LOD) [21] is used. This parameter is related to the signal to noise ratio (SNR) [22]: the signal depends on G_{SERS} but also on the type of analyte (through its cross section), on the sensitivity of the instrumentation (that is determined for example by the reflectance / transmittance of the optical components, the quantum efficiency of the detector and the collection geometry), on the laser power / intensity and on the integration time. In general, it is expected that G_{SERS} and the SERS signal have a different wavelength dependence: therefore, working in the spectral region where the substrate possesses the maximum G_{SERS} does not nec-

* Corresponding author at: Consorzio INSTM, Via G. Giusti 9, 50121 Firenze, Italy.
E-mail addresses: roberto.pilot@unipd.it (R. Pilot), michele.massari@unipd.it (M. Massari).
Present affiliation: ECSIN-European Center for the Sustainable Impact of Nanotechnology, EcamRicert srl, Mérieux NutriSciences, Corso Stati Uniti 4, 35127, Padova (Italy).

[1] The enhancement actually depends also on the polarization of the light source and on the geometry with which surface plasmons are excited. Concerning the polarization, its type and orientation are not critical if the substrate is a random surface; on the other hand, if the substrate possesses a long range order the excitation conditions should be declared. As for the geometry, in standard SERS experiments the illumination and collection are almost always accomplished perpendicularly to the sample in a back scattering configuration. Overall, for the wide majority of SERS experiments it is reasonable to assume that the polarization and excitation geometry issues are either not critical or clearly declared and therefore reproducible in different laboratories: these considerations support the assumption above that G_{SERS} depends principally on the type of material and on the morphology of the substrate.

https://doi.org/10.1016/j.chphi.2021.100014
Received 22 September 2020; Received in revised form 29 December 2020; Accepted 24 February 2021

essarily imply that the SERS measurement is carried out with the highest sensitivity (i.e. lowest detection limit).

The SERS properties of substrates are not very often reported as a function of the excitation wavelength, probably because the experimental apparatus required for this type of measurements is quite complex [23,24]: typically, multiline or tunable laser sources are used to excite the sample and the separation of the Raman scattering from the elastic scattering is accomplished by means of triple spectrographs. Nevertheless, the knowledge of the wavelength dependence of G_{SERS}, for example, is very useful to phenomenologically figure out where the substrate is more suitable for amplifying the optical signals or, conversely, it can be exploited to carry out structure-properties relations aimed to tune the plasmonic response in the desired region. The near infrared region (NIR) is extremely important for biomedical applications, since in this case the excitation has to be performed where the absorption / scattering of tissues is minimized: the first transparency window of biological tissues lies in between 650 and 950 nm (NIR-I), while the other two are located from 1000 to 1350 nm (NIR-II) and from 1550 to 1870 nm (NIR-III) [1,25]. NIR-I is the easiest to access with standard Raman instruments; NIR-II can be exploited for example with Fourier Transform Raman instruments equipped with 1064 nm lasers and Indium Gallium Arsenide (InGaAs) detectors [22]; NIR-III is rarely exploited to the best of our knowledge [22,26,27]. The excitation in the NIR is also very helpful to mitigate photobleaching and the fluorescent background generated by the compound under investigation or by impurities: owing to these features, (especially portable) Raman instruments equipped with NIR excitation are becoming more and more popular in the market [28].

In the following, a quick overview of the main contributions found in the literature on the wavelength dependence of G_{SERS} is presented both for NPs deposited on a surface (solid substrates) and for NPs in solution. In the framework of structure-property relationships, some studies have investigated whether far field spectra (scattering or extinction) and the near field spectra (probed through G_{SERS}) present some relation that could allow one to predict the latter (more difficult to measure experimentally) from the former (easier to determine). For example, McFarland et al. [23] studied an hexagonal array of Ag nanoprisms in the range 425–800 nm, showing that the extinction and G_{SERS} are closely correlated. Conversely, in single Au NP dimers and trimers embedded in a silica shell, Kleinman et al. [29] demonstrated that the G_{SERS} peak is strongly red shifted compared to the scattering peak. This study was carried out from 575 to 870 nm and the different behavior, compared to the paper by McFarland et al. [23], was attributed to the stronger coupling among NPs in the sample. Kurouski et al. [30] investigated samples formed by Au NPs, with different shapes and sizes, deposited on cellulose based polymeric fibers from 633 nm to 825 nm: with the help of finite difference time domain (FDTD) calculations the authors tried to correlate the morphology of the aggregated NPs with the observed far and near field spectra. Similar studies were carried out for example by Roy et al. [31] on aggregated Au NPs at 488, 532, 633, and 785 nm, by D'Andrea et al. [32] on a random array of Au NPs from 525 nm to 900 nm, and by Doherty et al. [33] on an ordered array of vertically aligned Au nanopillars from 532 nm to 780 nm. A specific type of aggregates, fractals, has also been subject of intense study: in particular Poliakov et al. [34] and Shalaev et al. [35] simulated G_{SERS} of self affine (from 200 to 1800 nm) and self similar (from 200 to 1100 nm) fractals made of spherical Ag NPs, respectively: the details of the method they used are reported in the book by Shalaev [36]. Experimental G_{SERS} spectra of fractal aggregates of Ag NPs have been carried out by Vlčková et al. [37], in the range 468–647 nm. Fractals made of spherical Au NPs have been studied by Das et al. [38] at 514 and 633 nm.

As for NPs in solution, Becucci et al. [39] have reported on the relative G_{SERS} of Ag nanowires with a high aspect ratio, at 407 nm, at 514 nm and at 1064 nm; in addition, the absorption and scattering components of the extinction were separated by means of photoacoustic spectroscopy. The far and near field properties were studied also by Weber et al. [40] for silica-gold core-shell NPs in the range 568–920 nm and by Zoppi et al. [24] for silver-gold nanocages between 568 and 810 nm. Several studies are available on spherical Ag NPs aggregated in solution, with G_{SERS} spectra collected up to approximately 700 nm [41–44] or in the NIR at 785 nm and 1064 nm [45].

Most of the above mentioned studies are limited to relatively short ranges of wavelengths and/or comprise a number of points (excitation wavelengths) not always high enough to clearly identify a trend.

In this paper, we have chosen to investigate Ag NP aggregates deposited on a surface: owing to their facility of preparation and good response they are very often used in SERS applications. Despite their popularity, to the best of our knowledge, the characterization of their SERS properties in a spectral range (680–920 nm) wide enough to cover most of NIR-I with a large number of excitation wavelengths is still missing. In particular, we have measured as a function of the excitation wavelength: a) the relative G_{SERS} and b) the SERS signal normalized by the laser power and by the integration time. Point a) is aimed to show how far in the NIR simple Ag NP aggregates are efficient plasmonic enhancers. The comparison of trends a) and b) provides a specific example of how the two parameters considered may exhibit a different spectral dependence, with relevant implications in the design of a SERS experiment.

2. Experimental

2.1. Reagents

Silver nitrate, trisodium citrate, sodium chloride, benzenethiol and methanol were purchased from Sigma Aldrich. P/Bor Silicon (100) wafers were bought from Si-Mat.

2.2. Sample preparation

Silver NPs were synthesized according to the procedure described by Lee et al. [46]. Forty five mg of $AgNO_3$ were dissolved in 250 ml of deionized water in an Erlenmeyer flask equipped with a reflux condenser and brought to boiling; 5 ml of a 1% solution of sodium citrate were added; after 1 h, the heating was turned off and the solution was left to cool down to room temperature. A microscopy slide was put at the bottom of a 50 ml beaker and 7 ml of the NP solution were poured inside; aggregation was induced by adding 1.2 ml of a 0.5 M solution of NaCl. The aggregation of the sample started shortly after the addition of salt as evidenced by the change in color of the solution; aggregates spontaneously separated from the solution and deposited on the microscopy slide overnight, leaving a transparent supernatant. Most of the water was delicately removed with a Pasteur pipette and the rest was let evaporate freely. Smaller NaCl solution volumes (1.0 and 0.5 ml) produced only a partial precipitation of the NPs, while with 0.1 ml no precipitation occurred. All measurements presented in this paper have been carried out on the sample precipitated with 1.2 ml of 0.5 M NaCl, except for the extinction spectra that have been recorded also for the preparations with 1.0 and 0.5 ml (Fig. S1).

The aggregates attached to the slide surface were functionalized by (overnight) immersion in a 10 mM solution of benzenethiol in methanol: the excess thiol was removed by thoroughly rinsing the sample with methanol.

2.3. Morphological characterization

Images of the sample were collected with an optical microscope (BX41, Olympus) and with a Schottky field emission scanning electron microscope (FE-SEM), FEI Nova 600-i NanoLab.

2.4. Optical characterization

Extinction spectra were collected with a Varian Cary 5 spectrometer in a 1 mm thick quartz cuvette.

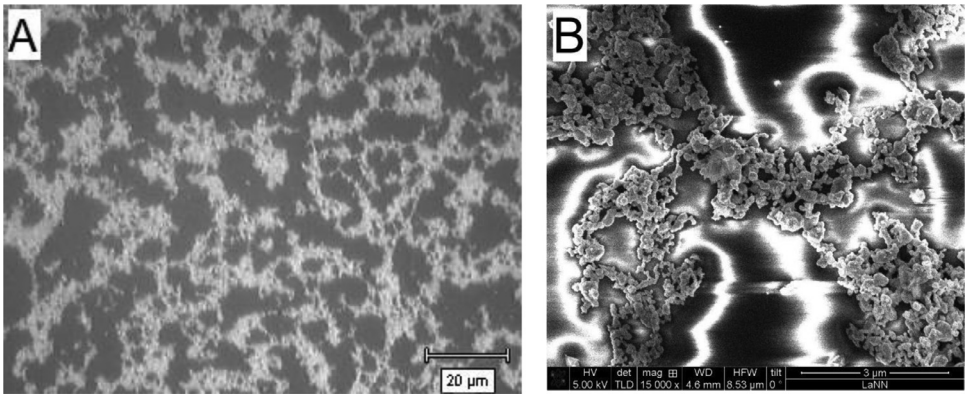

Fig. 1. A. Optical Image of the Ag NP aggregates. **B.** FE-SEM image of the Ag NP aggregates.

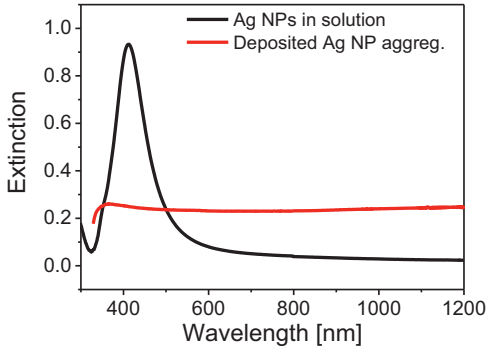

Fig. 2. Extinction spectrum of Ag NPs in solution (black line) and of the Ag NP aggregates deposited on the microscopy slide (red line). (For interpretation of the references to color in this figure legend, the reader is referred to the web version of this article.)

A home built MacroRaman setup, similar to the one used in previous publications [24,47,48], was used to carry out Raman measurements. In brief, the excitation in the NIR is provided by a continuous wave (CW) titanium-sapphire laser tunable in the range 675–1000 nm (3900S, Spectra Physics), pumped by a semiconductor laser (Verdi G7, Coherent). The laser is focused on the sample by a cylindrical lens: the laser spot is about 5 mm tall and 100 μm wide. The Raman signal is collected with a camera objective (CANON 50 mm, f/1.2) in a back scattering configuration. A three stage subtractive spectrograph (S3000, Jobin Yvon) is used to separate the Raman from the Rayleigh scattering. The detector (Symphony, Jobin Yvon) is a liquid nitrogen cooled charge coupled device (CCD).

The power impinging on the sample was in between 4 and 27 mW at all excitation wavelengths, which approximately corresponds to a laser intensity in the range of 1 to 5 W/cm^2.

The pure liquid benzenethiol was measured in a vial.

3. Results and discussion

3.1. Morphological characterization

Fig. 1 shows two images of the Ag NP aggregates on glass taken with an optical microscope (Fig. 1A) and with a FE-SEM (Fig. 1B). Large aggregates with a ramified structure are present on the surface.

3.2. Extinction measurements

The extinction spectrum of colloidal Ag NPs (black line) and the extinction spectrum of the deposited aggregates (red line) are shown in Fig. 2. Ag NPs in solution present a typical peak at 408 nm corresponding to the dipolar plasmonic resonance, while Ag NP aggregates exhibit a smooth extinction spectrum throughout the spectral region explored. Numerical data of all Figures in this paper (except for Figure 1) are reported in the supplementary material section.

3.3. SERS measurements

3.3.1. SERS enhancement

G_{SERS} is typically worked out with the following expression: [20,48]

$$G_{SERS} = \frac{P_{SERS}}{P_{Raman}} \frac{N_{Raman}}{N_{SERS}} \cong \frac{P_{SERS}}{P_{Raman}} \frac{C_V}{C_S} \frac{1}{A_{eff}} \eta^N \quad (1)$$

P_{SERS} and P_{Raman} are the integrated intensities of the 999 cm^{-1} Raman band of benzenethiol in the SERS experiment (benzenethiol on Ag NP aggregates) and in the normal Raman experiment (liquid benzenethiol in a vial), respectively: they are measured with the same setup, laser power and integration time. N_{SERS} and N_{Raman} are the number of molecules illuminated in the SERS and in the normal Raman experiment. When the numbers of illuminated molecules are rewritten as a function of the experimental parameters, G_{SERS} can be recast as indicated in the right hand term of Eq. (1). C_V is the number of molecules per cm^3 in the liquid benzenethiol; C_S is the number of benzenethiol molecules per cm^2 adsorbed on a flat Ag surface: both are known from the literature [23,47]. The constant A_{eff} accounts for the effect of the sample geometry on the number of illuminated molecules: for a flat Ag surface A_{eff}=1, but SERS samples have always complex morphologies and therefore A_{eff} can significantly differ from this value. η^N is the integrated area of the normalized collection efficiency, $\eta^N(Z)$, with respect to the propagation direction of the laser, Z: $\eta^N = \int_{-\infty}^{+\infty} \eta^N(Z) dZ$. $\eta^N(Z)$ is experimentally determined by recording the intensity of the 520 cm^{-1} Raman band of silicon at different positions along Z [20,48].

Absolute values of G_{SERS} are often difficult to determine, mainly because the estimation of the parameter A_{eff} is not trivial for substrates with a complex morphology like Ag NP aggregates. However, in order to study the wavelength dependence, it suffices to refer to G_{SERS} normalized to its maximum value, N_G_{SERS}. Since the term $\frac{C_V}{C_S}\frac{1}{A_{eff}}$ does not depend on the excitation wavelength, the parameters required to work out N_G_{SERS} are only P_{SERS} , P_{Raman} and η^N: as an example, we report the determination of these parameters at λ_{ex}= 750 nm. In Fig. 3A, a Raman and a SERS spectrum are shown. The main bands of benzenethiol in the SERS experiment have been assigned as follows[49]: 418 cm^{-1} (7a(a$_1$), $\upsilon_{CS} + \beta_{CCC}$), 692 cm^{-1} (6a(a$_1$), $\beta_{CCC} + \upsilon_{CS}$), 999 cm^{-1} (12(a$_1$), β_{CCC}), 1022 cm^{-1} (18a(a$_1$), β_{CH}), 1071 cm^{-1} (1(a1), $\beta_{CCC} + \upsilon_{CS}$), 1574 cm^{-1} (8a(a1), υ_{CC}). In parenthesis the corresponding Wilson mode of benzene, the symmetry and the mode composition are indicated: υ corresponds to the stretching and β to the in plane bending modes. In order to determine the area of the 999 cm^{-1} band, the two closely lying peaks at 999 cm^{-1} and 1022 cm^{-1} have been fitted with two Voigt functions (spectra have been previously baseline subtracted),

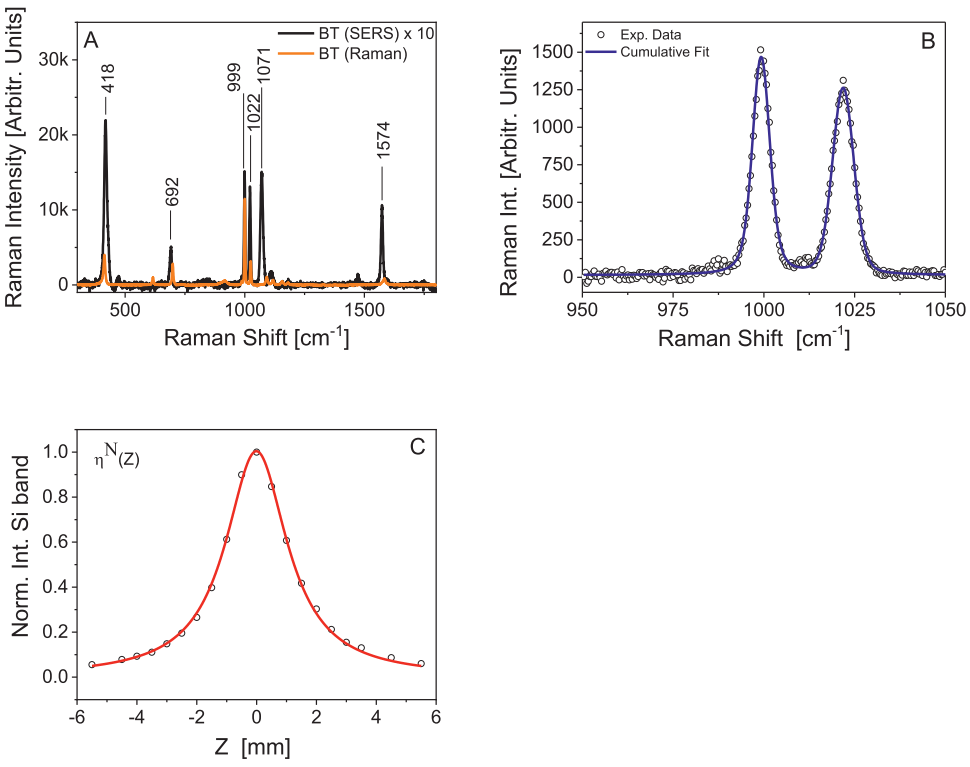

Fig. 3. A. SERS spectrum of benzenethiol on Ag NP aggregates (black line) and Raman spectrum of pure liquid benzenethiol (orange line). The SERS spectrum has been multiplied by 10 for displaying purposes. BT = benzenethiol. Experimental conditions: λ_{ex}=750 nm, laser power 8 mW, the spectrum is the average of 4 spectra (each with an integration time of 10 s). **B** Enlargement of the SERS spectrum of Fig. 3A in the region of the 999 cm^{-1} peak (not multiplied by 10). The empty dots are the experimental data and the blue line is the cumulative fit. Experimental conditions: λ_{ex}=750 nm, laser power 8 mW, the spectrum is the average of 4 spectra (each with an integration time of 10 s). **C** Experimental normalized collection efficiency, $\eta^N(Z)$, at λ_{ex}=750 nm. The intensity of the 520 cm^{-1} band of silicon is reported as a function of its position along the propagation direction of the laser, Z (empty dots): data are normalized to the maximum, Z=0, and fitted with a Lorenzian curve (red line). (For interpretation of the references to color in this figure legend, the reader is referred to the web version of this article.)

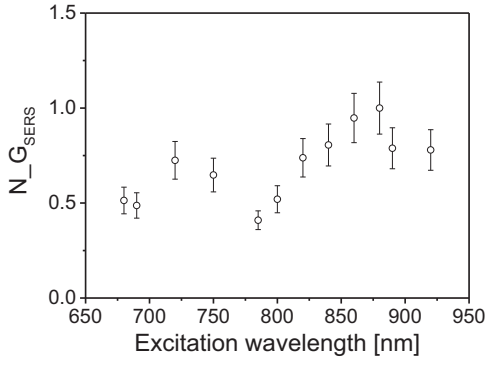

Fig. 4. N_G_{SERS} as a function of the excitation wavelength.

both for the normal Raman and for the SERS spectra. In Fig. 3B, an example of the fitting of a SERS spectrum is reported: only the cumulative fitting (blue line) is shown. The corresponding fittings of the 999 cm^{-1} and of the 1022 cm^{-1} peaks are shown in Figure S2. The collection efficiency $\eta^N(Z)$ is reported in Fig. 3C: it has been fitted with a Lorenzian curve to determine the integrated area η^N. N_G_{SERS} is reported in Fig. 4 as a function of the excitation wavelength: data are normalized at 880 nm. The homogeneity of the sample was tested at λ_{ex}= 785 nm by measuring the SERS signal at 14 different points: the relative standard deviation turned out to be 14%. Due to the very large laser spot area and to the intrinsic large spatial average associated, at the other wavelengths only 1 or 2 points were measured. At all wavelengths, both for N_G_{SERS} and for the normalized SERS signal presented in the next section, the error bar has been assumed to correspond to the relative standard deviation measured at λ_{ex}= 785 nm. Raw spectra and the data analysis are reported in the supplementary material section. Also the sample stability at laser exposure has been tested at 785 nm: two consecutive spectra were recorded at the same point of the substrate, irradiating it with the highest laser power used in the SERS experiments (27 mW). The spectra, reported in Fig. S3, look very similar and no signs of degradation are present.

Finally, although providing an absolute number for G_{SERS} is very challenging, we think that the following rule of thumb considerations may help figure out that the Ag NP aggregates possess a significant enhancement.

One option is considering simply $A_{eff} = 1$ in Eq. (1): this is equivalent to say that the roughness of the aggregates causes an increase of active surface (compared to a flat surface) that compensates for the areas on the sample not covered by NPs. G_{SERS} would amount to $\sim 4 \cdot 10^7$ (with $C_S = 6.8 \cdot 10^{14}\ \frac{molecules}{cm^2}$ and $C_V = 5.88 \cdot 10^{21}\ \frac{molecules}{cm^3}$ [23,47]). This value is pretty high, since Etchegoin et al. [50] have commented that a G_{SERS} of $10^7 - 10^8$ would be sufficient for single molecule detection of resonant molecules.

Another option is to compare the signal of Ag Np aggregates with the signal of a substrate whose enhancement is known: in Michieli et al. [47] a silver nanotriangle array functionalized with benzenethiol has been investigated using an experimental equipment very similar to the one used in this paper. Since the array possesses a controlled geometry, the number of illuminated molecules and the absolute G_{SERS} was worked out. The peak at 999 cm^{-1} in the SERS spectrum reported in Fig. 3a of Michieli et al. [47] has an intensity (height) of about 90 $\frac{Arbitr.Units}{mW \cdot s}$ (λ_{ex}= 710 nm), while the SERS spectra of Ag NP aggregates in Fig. 5A (this paper) have an intensity (height) of about 90 $\frac{Arbitr.\ Units}{mW \cdot s}$ (λ_{ex}= 680 nm) or 20 $\frac{Arbitr.\ Units}{mW \cdot s}$ (λ_{ex}= 750 nm). Therefore, Ag NP aggregates exhibit a SERS signal comparable to the signal measured for the nanotriangle array, that possesses a G_{SERS} of about $4 \cdot 10^6$ at 710 nm.

On the basis of the previous considerations, it seems reasonable to deduce that the plasmonic response of Ag NP aggregates is significant, although a precise number cannot be provided without knowing the number of illuminated molecules on the aggregates.

3.3.2. Normalized SERS signal

As an example, Fig. 5A shows three SERS spectra, recorded at λ_{ex}=680 nm (black line), λ_{ex}=750 nm (red line) and λ_{ex}=920 nm (green line), normalized by the laser power (in mW) and by the integration

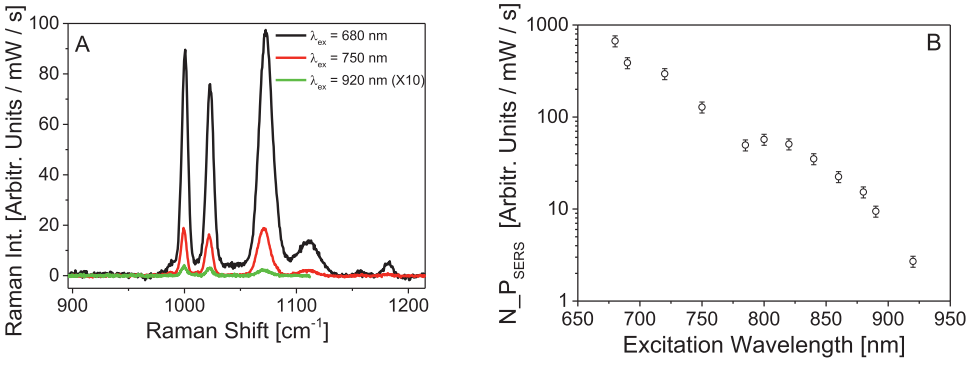

Fig. 5. A. SERS spectra normalized by the laser power (in mW) and by the integration time (in seconds) at λ_{ex}=680 nm (black line), λ_{ex}=750 nm (red line) and λ_{ex}=920 nm (green line). Spectrum at λ_{ex}=680 nm: laser power 6 mW, the spectrum is the average of 4 spectra (each with an integration time of 10 s); spectrum at λ_{ex}=750 nm: laser power 8 mW, the spectrum is the average of 4 spectra (each with an integration time of 10 s); spectrum at λ_{ex}=920 nm: laser power 10 mW, the spectrum is the average of 3 spectra (each with an integration time of 50 s) **B.** Integrated intensity of the 999 cm^{-1} SERS peak of benzenethiol normalized by the laser power (in mW) and by the integration time (in seconds), N_P_{SERS}, as a function of the excitation wavelength. (For interpretation of the references to color in this figure legend, the reader is referred to the web version of this article.)

Table 1
Overview of the literature papers in which the G_{SERS} wavelength dependence of solid substrates has been experimentally investigated. Only the papers by Poliakov et al. [34] and by Shalaev et al. [35] are purely theoretical contributions. The papers reported in this table correspond to those cited in the introduction.

Substrate	SERS λ_{ex} [nm]	Reference
Hexagonal array of nanoprisms	425–800	McFarland et al. [23]
Single dimers Au NPs embedded in a silica shell	575–870	Kleinman et al. [29]
Au NPs on polymeric fibers	633–825	Kurouski et al. [30]
Au NP aggregates	488, 532, 633, and 785	Roy et al. [31]
Random array of Au NPs	525–900	D'Andrea et al. [32]
Ordered array of vertically aligned Au nanopillars	532–780	Doherty et al. [33]
Aggregated Au NPs, Ag NPs, Au core – Ag shell NPs	514, 633	Das et al. [38]
Ag NP fractals	468–647	Vlčková et al. [37]
Ag NP fractals (self affine) - Simulations	200–1800	Poliakov et al. [34]
Ag NP fractals (self similar) - Simulations	200–1100	Shalaev et al. [35]
Ag NP aggregates	680–920	This paper

time (in seconds) to help the comparison among them. Fig. 5B reports the integrated area of the 999 cm^{-1} band of benzenethiol normalized as mentioned above, $N\_P_{SERS} = \frac{P_{SERS}\ (999\ cm^{-1})}{LaserPower \cdot Integr.\ Time}[\frac{Arbitr.\ Units}{mW \cdot s}]$, as a function of the excitation wavelength; In Fig. S4, $N\_P_{Raman} = \frac{P_{Raman}\ (999\ cm^{-1})}{LaserPower \cdot Integr.\ Time}[\frac{Arbitr.\ Units}{mW \cdot s}]$ is reported as well.

4. Discussion

4.1. Wavelength dependence of N_G$_{SERS}$

The trend of N_G_{SERS} reported in Fig. 4 indicates that Ag NP aggregates can enhance the local field in most of the first transparency window NIR-I, that lies between 650 and 980 nm. Table 1 summarizes a number of studies that deal with the G_{SERS} dependence on the excitation wavelength of solid substrates.

Concerning the shape of N_G_{SERS}, it does not show a significant wavelength dependence.

It is known that the interaction among NPs leads to a red shift of the local field maximum compared to the isolated NPs [51]. Etchegoin et al. [52] clearly showed this effect for a dimer of spherical NPs by means of the generalized Mie theory: in this case, the maximum of G_{SERS} moved approximately from 420 nm (single Ag NP, 25 nm radius) to 450 nm (dimer of Ag NPs with 20 nm gap) and to 600 nm (dimer of Ag NPs with 1 nm gap). SERS experiments at several excitation wavelengths have been carried out by Kleinman et al. [29] on single nanoantennas formed by Au NP dimers, trimers or higher order structures embedded in a silica shell: measurements showed that in these samples G_{SERS} reaches very high values in between 700 and 900 nm. Kurouski et al. [30] investigated three substrates formed by Au NPs of different size and shape deposited on cellulose based polymeric fibres. SERS measurements revealed that G_{SERS} increases by 5–10 times from 625 nm to 825 nm for all substrates: however, in the samples loaded with spherical NPs, it reaches a maximum or a plateau, depending on the size of the NPs, while in the sample loaded with nanorods the trend rises more steeply and suggests further growth above 825 nm. These red shifted and broad G_{SERS} spectra, on the basis of the SEM images and of the FTDT simulations, have been associated to the presence of NP clusters, mainly dimers and trimers. In view of the papers discussed above, it seems reasonable that the weak wavelength dependence of N_G_{SERS} arises from the variety of geometries and gap dimensions in which Ag NPs are probably arranged in the large sized aggregates.

An additional key of interpretation could be found in the context of fractals, which are scale invariant objects that look similar at increasingly small scales (when the scaling properties are the same along all directions one refers to self similar objects, while when the scaling properties in the xy plane are different from the ones along z, one refers to self affine objects [36]). Fractals can be fabricated by inducing controlled aggregation of colloidal solutions of Ag or Au NPs. If, for example, a salt is added to a colloidal solution of NPs, the increased ionic strength reduces the electrostatic screening among the NPs allowing them to stick together upon collision. Aggregates can slowly grow until, due to their size, they precipitate from the solution. The resulting fractal is a tenuous ramified structure containing closely lying NPs [36,37,53]; deposited fractals are normally self affine structures [36]. The Ag NP aggregates prepared in this paper may exhibit some fractal properties. In fact, the optical and FE-SEM images reported in Fig. 1 reveal a ramified structure that closely resembles the fractal aggregates reported by Vlčková et al. [37] and by Markel et al. [53]; moreover, it is worth noticing that the aggregation of NPs in this paper is accomplished by addition of NaCl and occurs slowly, over several hours, similarly to the preparation method mentioned above. Vlčková et al. [37] measured the SERS profile of fractal aggregates in the range 468–647 nm. Data are compatible with an

increase of the enhancement towards the red, although the generation of photoproducts of the analyte phthalazine (more pronounced with the shorter excitation wavelengths) caused some Raman bands to exhibit non monotonically growing profiles. Optical properties of Ag NP fractals have also been studied in a wider range by means of simulations. Poliakov et al. [34] predicted, for self affine fractals, a rise of G_{SERS} from 400 to 700 nm and only a minimal wavelength dependence from 700 nm to 1800 nm. In conclusion, the preparation method and the FE-SEM / optical images suggest that Ag NP aggregates could possess a fractal nature; moreover, the G_{SERS} spectrum predicted by Poliakov et al. [34] agrees well with the experimental measurements reported in this paper.

4.2. *Wavelength dependence of* N_P$_{SERS}$

The trend of N_P_{SERS} reported in Fig. 5B, despite N_G_{SERS}, shows a strong dependence on the excitation wavelength: it undergoes a reduction by a factor of about 200 from 680 to 920 nm. This happens because N_P_{SERS} depends on the enhancement but also on the cross section of the molecule and on the instrument sensitivity. In the following, the wavelength dependence of the cross section and of the instrument sensitivity are briefly analyzed. The Raman cross section of the k-th mode of a molecule can be expressed as[22]:

$$\sigma_k \propto \tilde{\nu}_0\left(\tilde{\nu}_0 - \tilde{\nu}_k\right)^3 \sim \tilde{\nu}_0^4 \tag{2}$$

where $\tilde{\nu}_0$ is the excitation laser wavenumber, $\tilde{\nu}_k$ is the Raman shift of the mode k, and $\tilde{\nu}_0 - \tilde{\nu}_k$ is the absolute (Stokes) Raman wavenumber. In first approximation, for small Raman shifts, the frequency dependence can be written as $\sim \tilde{\nu}_0^4$. Eq. (2) shows that the longer the excitation wavelength, the lower the cross section: for example, considering $\tilde{\nu}_k = 1000$ cm^{-1} (i.e. the trigonal mode of benzenethiol), the relative cross sections at $\lambda_{Exc} = 680, 750, 920$ nm turn out to be $\sigma(680\ nm) : \sigma(750\ nm) : \sigma(920\ nm) = 1 : 0.66 : 0.28$. Therefore, working at 920 nm, rather than at 680 nm, implies a 4-fold decrease of signal due to a reduction of the cross section. Concerning the instrument sensitivity, the two components that are more important are the gratings and the CCD detector. The grating reflectivity can be optimized for working in different spectral ranges; however, in dispersive instruments like the one we used in our experiments, the CCD chip is made of silicon and its quantum efficiency quickly diminishes when the wavelength approaches its band gap that is around 1100 nm (above the band gap silicon is transparent and no photoelectrons would be generated) [54]. It is worth noticing that when working at the longest excitation wavelength, 920 nm, the absolute wavelength of a Raman mode at 1000 cm^{-1} is already 1013 nm and the absolute wavelength of a mode at 3000 cm^{-1} (i.e. the region of C–H stretching) is 1270 nm.

Concerning the SNR, in shot noise limited experiments, it can be expressed by the relation $SNR = \frac{S}{\sqrt{S+B}}$, where S is the signal above the background and B is the background [22]. Assuming that B is low (reasonable for non fluorescent molecules like benzenethiol), $SNR \cong \sqrt{S}$. This shows that the reduction of N_P_{SERS} by 200 times going from 680 nm to 920 nm brings about a reduction of the SNR, and hence of the LOD, by $\sqrt{200} \cong 14$ times (supposing that the SERS spectra have been recorded with the same laser power and integration time).

Therefore, the combined effect of the cross section and of the instrument sensitivity tends to significantly reduce the signal at longer excitation wavelengths.

4.3. *Final considerations*

The comparison of N_G_{SERS} (Fig. 4) and N_P_{SERS} (Fig. 5B) shows that the substrate enhancement and the sensitivity of the measurement can exhibit remarkably different wavelength dependences. Actually, both parameters are important in the engineering of a SERS experiment since the former is a characteristic proper of the substrate, that should be independent of the laboratory in which it is measured, while the latter is more closely related to the LOD, that is the relevant parameter for analytical applications of SERS.

The observation that the normalized signal decreases towards the red should be quite general for non resonant molecules and dispersive instruments equipped with silicon detectors. Things would be of course different with resonant molecules or with instruments designed for working specifically in the NIR (i.e. Fourier transform instruments with InGaAs detectors).

5. Conclusions

In this paper, Ag NP aggregates have been prepared by adding NaCl to a colloidal solution of Ag NPs: the slow coalescence of NPs led to the formation of large aggregates that separated from the solution. The morphology of these aggregates, deposited on a glass slide, was characterized by optical and FE-SEM microscopy. The relative SERS enhancement and the SERS signal normalized by laser power and integration time were measured from 680 nm to 920 nm.

The main findings of this paper can be summarized as follows:

- Ag NP aggregates show a significant SERS enhancement from 680 to 920 nm, therefore in most of the first transparency window of biological tissues.
- The relative SERS enhancement has a weak wavelength dependence.
  - We hypothesize that, being the aggregates very large, the NPs are arranged in many complex geometries with different gaps, leading to a large broadening of the plasmonic response. In addition, optical and FE-SEM images show that Ag NP aggregates could have a fractal character: literature simulations on self affine fractals show that relative SERS enhancement does not vary significantly in the NIR, consistently with experimental data reported in this paper.
- The normalized SERS signal shows a strong reduction, of about 200 times, going from 680 nm to 920 nm.
  - This signal reduction has been attributed to its dependence on the Raman cross section and on the instrument sensitivity. The cross section of a non resonant molecule scales with the forth power of the excitation frequency; the sensitivity of an instrument equipped with a silicon CCD detector quickly diminishes when the photon wavelength approaches the silicon band gap, located at 1100 nm.
- The relative SERS enhancement and the normalized SERS signal exhibit remarkably different wavelength dependences, showing that the sensitivity of a measurement is not simply related to the substrate enhancement. Both parameters have to be taken into account in the design of a SERS experiment.

Declaration of Competing Interest

The authors declare that they have no known competing financial interests or personal relationships that could have appeared to influence the work reported in this paper.

Acknowledgments

Financial support by Ministero dell'Istruzione, dell'Università e della Ricerca (MIUR) through the FIRB project ITALNANONET (RBPR05JH2P_001) is gratefully acknowledged.

Supplementary materials

Supplementary material associated with this article can be found, in the online version, at doi:10.1016/j.chphi.2021.100014.

References

[1] R. Pilot, R. Signorini, C. Durante, L. Orian, M. Bhamidipati, L. Fabris, A review on surface-enhanced Raman scattering, Biosensors 9 (2019) 57, doi:10.3390/bios9020057.

[2] R. Pilot, R. Signorini, L. Fabris, Surface-enhanced Raman spectroscopy: principles, substrates, and applications, in: F.L. Deepak (Ed.), Met. Nanoparticles Clust. Adv. Synth. Prop. Appl., Springer, Cham, 2018, pp. 89–164, doi:10.1007/978-3-319-68053-8_4.

[3] J. Langer, D.J. de Aberasturi, J. Aizpurua, R.A. Alvarez-Puebla, B. Auguié, J.J. Baumberg, G.C. Bazan, S.E.J. Bell, A. Boisen, A.G. Brolo, J. Choo, D. Cialla-May, V. Deckert, L. Fabris, K. Faulds, F. Javier García de Abajo, R. Goodacre, D. Graham, A.J. Haes, C.L. Haynes, C. Huck, T. Itoh, M. Käll, J. Kneipp, N.A. Kotov, H. Kuang, E.C. Le Ru, H.K. Lee, J.F. Li, X.Y. Ling, S.A. Maier, T. Mayerhöfer, M. Moskovits, K. Murakoshi, J.M. Nam, S. Nie, Y. Ozaki, I. Pastoriza-Santos, J. Perez-Juste, J. Popp, A. Pucci, S. Reich, B. Ren, G.C. Schatz, T. Shegai, S. Schlücker, L.L. Tay, K. George Thomas, Z.Q. Tian, R.P. van Duyne, T. Vo-Dinh, Y. Wang, K.A. Willets, C. Xu, H. Xu, Y. Xu, Y.S. Yamamoto, B. Zhao, L.M. Liz-Marzán, Present and future of surface-enhanced Raman scattering, ACS Nano 14 (2020) 28–117, doi:10.1021/acsnano.9b04224.

[4] R. Pilot, SERS detection of food contaminants by means of portable Raman instruments, J. Raman Spectrosc. 49 (2018) 954–981, doi:10.1002/jrs.5400.

[5] A. Feis, C. Gellini, M. Ricci, L. Tognaccini, M. Becucci, G. Smulevich, Surface-enhanced Raman scattering of glyphosate on dispersed silver nanoparticles: a reinterpretation based on model molecules, Vib. Spectrosc. 108 (2020) 103061, doi:10.1016/j.vibspec.2020.103061.

[6] F. Zapata, M. López-López, C. García-Ruiz, Detection and identification of explosives by surface enhanced Raman scattering, Appl. Spectrosc. Rev. 51 (2015) 227–262.

[7] A. Hakonen, P.O. Andersson, M. Stenbæk Schmidt, T. Rindzevicius, M. Käll, Explosive and chemical threat detection by surface-enhanced Raman scattering: a review, Anal. Chim. Acta 893 (2015) 1–13, doi:10.1016/j.aca.2015.04.010.

[8] R. Gillibert, J.Q. Huang, Y. Zhang, W.L. Fu, M. Lamy de la Chapelle, Explosive detection by surface enhanced Raman scattering, Trends Anal. Chem. 105 (2018) 166–172, doi:10.1016/j.trac.2018.03.018.

[9] H. Wei, S.M. Hossein Abtahi, P.J. Vikesland, Plasmonic colorimetric and SERS sensors for environmental analysis, Environ. Sci. Nano 2 (2015) 120–135, doi:10.1039/c4en00211c.

[10] T.T.X. Ong, E.W. Blanch, O.A.H. Jones, Surface enhanced Raman spectroscopy in environmental analysis, monitoring and assessment, Sci. Total Environ. 720 (2020) 137601, doi:10.1016/j.scitotenv.2020.137601.

[11] F. Pozzi, M. Leona, Surface-enhanced Raman spectroscopy in art and archaeology, J. Raman Spectrosc. 47 (2016) 67–77, doi:10.1002/jrs.4827.

[12] I. Bruzas, W. Lum, Z. Gorunmez, L. Sagle, Advances in surface-enhanced Raman spectroscopy (SERS) substrates for lipid and protein characterization: sensing and beyond, Analyst 143 (2018) 3990–4008, doi:10.1039/c8an00606g.

[13] X.S. Zheng, I.J. Jahn, K. Weber, D. Cialla-May, J. Popp, Label-free SERS in biological and biomedical applications: recent progress, current challenges and opportunities, Spectrochim. Acta Part A Mol. Biomol. Spectrosc. 197 (2018) 56–77, doi:10.1016/j.saa.2018.01.063.

[14] E. Garcia-Rico, R.A. Alvarez-Puebla, L. Guerrini, Direct surface-enhanced Raman scattering (SERS) spectroscopy of nucleic acids: from fundamental studies to real-life applications, Chem. Soc. Rev. 47 (2018) 4909–4923, doi:10.1039/c7cs00809k.

[15] P.A. Mosier-Boss, Review on SERS of bacteria, Biosensors 7 (2017) 1–26, doi:10.3390/bios7040051.

[16] D. Cialla-May, X.-S. Zheng, K. Weber, J. Popp, Recent progress in surface-enhanced Raman spectroscopy for biological and biomedical applications: from cells to clinics, Chem. Soc. Rev. 46 (2017) 3857–4112, doi:10.1039/C7CS00172J.

[17] S.K. Das, K. Pal, T.S. Bhattacharya, P. Karmakar, J. Chowdhury, Fabrication of SERS active Langmuir–Blodgett Film substrate for screening human cancer cell lines: experimental observations supported by multivariate data analyses, Sens. Actuat. B Chem. 299 (2019) 126962, doi:10.1016/j.snb.2019.126962.

[18] T. Hartman, C.S. Wondergem, N. Kumar, A. Van Den Berg, B.M. Weckhuysen, Surface- and tip-enhanced Raman spectroscopy in catalysis, J. Phys. Chem. Lett. 7 (2016) 1570–1584, doi:10.1021/acs.jpclett.6b00147.

[19] M. Muniz-Miranda, Application of the SERS spectroscopy to the study of catalytic reactions by means of mono and bimetallic nanoparticles, J. Anal. Bioanal. Tech. 6 (2015) 1000286, doi:10.4172/2155-9872.1000286.

[20] E.C. Le Ru, E.J. Blackie, M. Meyer, P.G. Etchegoin, Surface enhanced Raman scattering enhancement factors: a comprehensive study, J. Phys. Chem. C 111 (2007) 13794–13803, doi:10.1021/jp0687908.

[21] S.E.J. Bell, G. Charron, E. Cortés, J. Kneipp, M.L. de la Chapelle, J. Langer, M. Procházka, V. Tran, S. Schlücker, Towards reliable and quantitative surface-enhanced Raman scattering (SERS): from key parameters to good analytical practice, Angew. Chem. Int. Ed. 59 (2020) 5454–5462, doi:10.1002/anie.201908154.

[22] R.L. McCreery, Raman Spectroscopy for Chemical Analysis, John Wiley & Sons, Inc., New York, USA, 2000, doi:10.1002/0471721646.

[23] A.D. McFarland, M.A. Young, J.A. Dieringer, R.P. Van Duyne, Wavelength-scanned surface-enhanced Raman excitation spectroscopy, J. Phys. Chem. B 109 (2005) 11279–11285, doi:10.1021/jp050508u.

[24] R. Pilot, A. Zoppi, S. Trigari, F.L. Deepak, E. Giorgetti, R. Bozio, Wavelength dispersion of the local field intensity in silver-gold nanocages, Phys. Chem. Chem. Phys. 17 (2015) 7355–7365, doi:10.1039/c4cp04453c.

[25] E. Hemmer, A. Benayas, F. Légaré, F. Vetrone, Exploiting the biological windows: current perspectives on fluorescent bioprobes emitting above 1000nm, Nanoscale Horiz. 1 (2016) 168–184, doi:10.1039/c5nh00073d.

[26] H. Kearns, M.A. Bedics, N.C. Shand, K. Faulds, M.R. Detty, D. Graham, Sensitive SERS nanotags for use with 1550nm (retina-safe) laser excitation, Analyst 141 (2016) 5062–5065, doi:10.1039/c5an02662h.

[27] C. Brouillette, H. Huang, W. Smith, S. Farquharson, Raman spectroscopy using 1550nm (retina-safe) laser excitation, Appl. Spectrosc. 65 (2011) 561–563, doi:10.1366/11-06232.

[28] K. Carron, R. Cox, Qualitative analysis and the answer box : a perspective on portable Raman spectroscopy, Anal. Chem. 82 (2010) 3419–3425, doi:10.1021/ac901951b.

[29] S.L. Kleinman, B. Sharma, M.G. Blaber, A.I. Henry, N. Valley, R.G. Freeman, M.J. Natan, G.C. Schatz, R.P. Van Duyne, Structure enhancement factor relationships in single gold nanoantennas by surface-enhanced Raman excitation spectroscopy, J. Am. Chem. Soc. 135 (2013) 301–308, doi:10.1021/ja309300d.

[30] D. Kurouski, N. Large, N. Chiang, N. Greeneltch, K.T. Carron, T. Seideman, G.C. Schatz, R.P. Van Duyne, Unraveling near-field and far-field relationships for 3D SERS substrates – a combined experimental and theoretical analysis, Analyst 141 (2016) 1779–1788, doi:10.1039/c5an01921d.

[31] S.D. Roy, M. Ghosh, J. Chowdhury, Near-field response on the far-field wavelength-scanned surface- enhanced Raman spectroscopic study of methylene blue adsorbed on gold nanocolloidal particles, J. Phys. Chem. C 122 (2018) 10981–10991, doi:10.1021/acs.jpcc.8b00315.

[32] C. D'Andrea, A. Irrera, B. Fazio, A. Foti, E. Messina, O.M. Maragò, S. Kessentini, P. Artoni, C. David, P.G. Gucciardi, C. D'Andrea, A. Irrera, B. Fazio, A. Foti, E. Messina, O.M. Maragò, S. Kessentini, P. Artoni, C. David, P.G. Gucciardi, Red shifted spectral dependence of the SERS enhancement in a random array of gold nanoparticles covered with a silica shell: extinction versus scattering, J. Opt. 17 (2015) 114016, doi:10.1088/2040-8978/17/11/114016.

[33] M.D. Doherty, A. Murphy, R.J. Pollard, P. Dawson, Surface-enhanced Raman scattering from metallic nanostructures: bridging the gap between the near-field and far-field responses, Phys. Rev. X 3 (2013) 1–12, doi:10.1103/PhysRevX.3.011001.

[34] E.Y. Poliakov, V.M. Shalaev, V.A. Markel, R. Botet, Enhanced Raman scattering from self-affine thin films, Opt. Lett. 21 (1996) 1628–1630.

[35] V.M. Shalaev, E. Poliakov, V. Markel, Small-particle composites. II. Nonlinear optical properties, Phys. Rev. B Condens. Matter Mater. Phys. 53 (1996) 2437–2449, doi:10.1103/PhysRevB.53.2437.

[36] V.M. Shalaev, Nonlinear Optics of Random Media. Fractal Composites and Metal-Dielectric Films, Springer-Verlag, Berlin Heidelberg GmbH, 2000, doi:10.1007/978-3-540-79572-8_1.

[37] B. Vlčková, X.J. Gu, M. Moskovits, SERS excitation profiles of phthalazine adsorbed on single colloidal silver aggregates as a function of cluster size, J. Phys. Chem. B 101 (1997) 1588–1593, doi:10.1021/jp961703z.

[38] S.K. Das, S. Saha, M. Ghosh, J. Chowdhury, How SERS responses of probe molecules depend on topographies of the substrates? A vis-à-vis exploration, Vib. Spectrosc. 107 (2020) 103031, doi:10.1016/j.vibspec.2020.103031.

[39] M. Becucci, M. Bracciali, G. Ghini, C. Lofrumento, G. Pietraperzia, M. Ricci, L. Tognaccini, S. Trigari, C. Gellini, A. Feis, Silver nanowires as infrared-active materials for surface-enhanced Raman scattering, Nanoscale 10 (2018) 9329–9337, doi:10.1039/c8nr00537k.

[40] V. Weber, A. Feis, C. Gellini, R. Pilot, P.R. Salvi, R. Signorini, Far- and near-field properties of gold nanoshells studied by photoacoustic and surface-enhanced Raman spectroscopies, Phys. Chem. Chem. Phys. (2014) 17, doi:10.1039/c4cp05054a.

[41] K.U. Von Raben, R.K. Chang, B.L. Laube, P.W. Barber, Wavelength dependence of surface-enhanced Raman scattering from Ag colloids with adsorbed CN- complexes, SO3, and pyridine, J. Phys. Chem. 88 (1984) 5290–5296.

[42] D. Fornasiero, F. Grieser, Analysis of the visible absorption and SERS excitation spectra of silver sols, J. Chem. Phys. 87 (1987) 3213, doi:10.1063/1.453009.

[43] M. Kerker, O. Siiman, O.S. Wang, Effect of aggregates on extinction and surface-enhanced Raman scattering spectra of colloidal silver, J. Phys. Chem. 88 (1984) 3168–3170, doi:10.1021/j150659a003.

[44] H. Feilchenfeld, O. Siiman, Surface Raman excitation and enhancement profiles for chromate, molybdate, and tungstate on colloidal silver, J. Phys. Chem. 90 (1986) 2163–2168.

[45] N. Leopold, B. Lendl, A new method for fast preparation of highly surface-enhanced raman scattering (SERS) active silver colloids at room temperature by reduction of silver nitrate with hydroxylamine hydrochloride, J. Phys. Chem. B 107 (2003) 5723–5727, doi:10.1021/jp027460u.

[46] P.C. Lee, D. Meisel, Adsorption and surface-enhanced raman of dyes on silver and gold sols, J. Phys. Chem. 86 (1982) 3391–3395, doi:10.1021/j100214a025.

[47] N. Michieli, R. Pilot, V. Russo, C. Scian, F. Todescato, R. Signorini, S. Agnoli, T. Cesca, R. Bozio, G. Mattei, Oxidation effects on the SERS response of silver nanoprism arrays, RSC Adv 7 (2017) 369–378, doi:10.1039/c6ra26307k.

[48] R. Pilot, R. Bozio, Validation of SERS enhancement factor measurements, J. Raman Spectrosc. 49 (2018) 462–471, doi:10.1002/jrs.5302.

[49] T.H. Joo, M.S. Kim, K. Kim, Surface-enhanced raman scattering of benzenethiol in silver Sol, J. Raman Spectrosc. 18 (1987) 57–60, doi:10.1002/jrs.1250221214.

[50] P.G. Etchegoin, E.C. Le Ru, A perspective on single molecule SERS: current status and future challenges, Phys. Chem. Chem. Phys. 10 (2008) 6079–6089, doi:10.1039/b809196j.

[51] V. Amendola, R. Pilot, M. Frasconi, O.M. Maragò, M.A. Iatì, Surface plasmon resonance in gold nanoparticles: a review, J. Phys. Condens. Matter. 29 (2017) 203002, doi:10.1088/1361-648X/aa60f3.

[52] E.C. Le Ru, P.G. Etchegoin, Principles of Surface Enhanced Raman Spectroscopy, Elsevier, Amsterdam, 2009.

[53] V.A. Markel, V.M. Shalaev, E.B. Stechel, W. Kim, R.L. Armstrong, Small-particle composites. I. Linear optical properties, Phys. Rev. B. 53 (1996) 2425–2436.

[54] N.W. Aschroft, N.D. Mermin, Solid State Phys. (1976).